Efficient Semi-Implicit Numerical Integration of ANCF and ALE-ANCF Cable Models with Holonomic Constraints

Cassidy Westin*, Rishad A. Irani

Department of Mechanical and Aerospace Engineering, Carleton University, 1125 Colonel By Drive, Ottawa, Canada, K1S 5B6

Abstract

In this paper, a method for integrating the equations of motion for Absolute Nodal Coordinate Formulation (ANCF) cable models using the Arbitrary Lagrangian-Eulerian (ALE) framework is described. The proposed semi-implicit method, based on a linearization of the generalized forces, eliminates the need for iterative solution methods required by implicit integrators and incorporates rigid holonomic constraints. Both the constraint forces and the generalized accelerations can be obtained in a single step using a linear solver greatly improving the computational efficiency. Four semi-implicit integrators are derived based on popular implicit methods. The paper examines the suitability of the four semi-implicit integrators for real-time cable simulations through three benchmark studies, comparing both the accuracy and computation speed of the method with the fully implicit Newmark method. The efficiency of the method is demonstrated by obtaining stable real-time simulations in each scenario considered.

Keywords: Cable simulation, Absolute Nodal Coordinate Formulation, Arbitrary Lagrangian Eulerian method, Time integration

*Corresponding author.

Email addresses: cassidy.westin@carleton.ca (Cassidy Westin), rishad.irani@carleton.ca (Rishad A. Irani)

1. Introduction

Dynamic simulations of flexible bodies such as cables and ropes enable engineers to examine their behavior under a variety of conditions. Real-time Finite Element (FE) simulations have been suggested [1] as a way to produce simulated data such as cable tension and displacement during an operation, eliminating the need for physical measurements; however, these real-time simulations have yet to be realized. In order to achieve a real-time FE simulation, both the FE model and the numerical integration method for incrementing the dynamic model at each time-step must be considered. This paper addresses the need for an efficient algorithm to achieve real-time simulations of flexible cables.

Various methods have been proposed to model flexible cables, including continuous mathematical models [2, 3], rigid body models [4], and discrete FE methods [5]. The Absolute Nodal Coordinate Formulation (ANCF) [6] is a popular nonlinear FE method which has been employed by numerous researchers to model various cable systems including marine towed cables [7, 8], cable-pulley systems [9, 10, 11], and mooring lines [12].

Hong et al. [13] proposed a generalization of the ANCF method which utilizes an Arbitrary-Lagrangian Eulerian (ALE) formulation. The ALE-ANCF decouples the motion of the cable material from the motion of the Finite Element mesh. Using the ALE method, element lengths can change dynamically and material can flow through fixed FE nodes. As a result, fewer elements are required to model complex cable systems such as cranes [14], reeving systems [15], and variable-length, deployable cables [16, 17]. In a trade study evaluating various cable modelling techniques, Fotland et al. [14] identify the ALE-ANCF as the most suitable option for creating a real-time simulation of a shipboard crane due to its efficiency, accuracy and the ability to dynamically vary the cable-length, however the method was not implemented by the researchers.

Few studies have examined simulating cables in real-time using ANCF and ALE-ANCF methods. One of the principal challenges in developing a real-time simulation is finding an appropriate numerical integration method. The

majority of numerical integration techniques can be described as either explicit or implicit. Explicit methods use only the system states at the current time-step to determine the states at the next time-step. For implicit methods, the solution is a function of the states at both the current and next time-steps.

In general, simulations of stiff bodies such as cables utilize implicit time-stepping equations which are solved using an iterative algorithm [18] as implicit methods often provide unconditional stability [19]. Implicit methods typically utilize a variable time-step in order to satisfy a user-specified error tolerance. Additionally, they require an iterative solution method, such as the Newton-Raphson algorithm, in order to solve the implicit time-stepping equations. Implicit methods are thus undesirable for real-time simulation as the computation time required to increment the model a certain period of time may vary significantly based on the number of iterations required at each time-step and the size of the time-step itself. Numerous studies have utilized implicit integrators for offline cable simulations. Fotland and Haugen [20] suggest the implicit fourth order Runge-Kutta and Generalized-α methods as potential integrators for real-time cable simulations using the ALE-ANCF method, however they do not report absolute computation times in their study.

Explicit integration methods, in contrast, are less computationally expensive than implicit methods, since the explicit equations can be solved in a single step without iteration, but typically have poor stability characteristics and often require very small time-steps [19]. Several semi-implicit methods have been developed in order to strike a balance between implicit and explicit methods by capturing the stability characters of fully implicit methods, while requiring only a single iteration per time-step.

1.1. Semi-Implicit Integration

Semi-implicit methods have been widely used in the computer graphics domain for simulating cloth and other flexible objects. A seminal method for simulating cloth proposed by Baraff and Witkin [21] stems from the implicit

Backward Euler (BE) method, given by the equations

$$\mathbf{q}_{n+1} = \mathbf{q}_n + h\mathbf{v}_{n+1} \tag{1a}$$

$$\mathbf{v}_{n+1} = \mathbf{v}_n + h\mathbf{M}^{-1}\mathbf{Q}(\mathbf{q}_{n+1}, \mathbf{v}_{n+1}) \tag{1b}$$

where $\mathbf{q}$ is a vector of generalized coordinates, $\mathbf{v} = \partial\mathbf{q}/\partial t$ is a vector of generalized velocities, h is the step size, $\mathbf{M}$ is the system mass matrix, $\mathbf{Q}$ is the vector of generalized coordinates. The subscript n represents the time-step.

In order to obtain an exact solution of Equation 1 an iterative algorithm, such as the Newton-Raphson method, is required. A more computationally efficient alternative proposed by Baraff and Witkin is to approximate the generalized forces $\mathbf{Q}$ at time-step $n+1$ using a Taylor series expansion,

$$\mathbf{Q}_{n+1} \approx \mathbf{Q}_n + \frac{\partial\mathbf{Q}}{\partial\mathbf{q}}(\mathbf{q}_{n+1} - \mathbf{q}) + \frac{\partial\mathbf{Q}}{\partial\mathbf{v}}(\mathbf{v}_{n+1} - \mathbf{v}_n), \tag{2}$$

which is substituted into Equation 1b to obtain

$$\left(\mathbf{M} - h\frac{\partial\mathbf{Q}}{\partial\mathbf{v}} - h^2\frac{\partial\mathbf{Q}}{\partial\mathbf{q}}\right)(\mathbf{v}_{n+1} - \mathbf{v}_n) = h\mathbf{Q}_n + h^2\frac{\partial\mathbf{Q}}{\partial\mathbf{q}}\mathbf{v}_n. \tag{3}$$

Using Equation 3, the generalized velocities $\mathbf{v}_{n+1}$ can be obtained in a single step and the generalized coordinates $\mathbf{q}_{n+1}$ can be found using Equation 1a.

A primary drawback of Baraff and Witkin's method is the presence of fictitious damping arising from the integrator itself rather than from the dynamic model. The amount of dissipation is tied to the time-step which can result in excessive attenuation of the motion and degrade the physical accuracy of the simulation when a large time-step is selected. Other researchers have proposed similar methods based on other implicit integration schemes in order to reduce the amount of dissipation. Choi and Ko [22] utilize the order-2 Backwards Differentiation Formula (BDF2), which exhibits less dissipation and similar stability as the order-1 BDF, which is synonymous with the implicit Euler method. Choi and Ko employ the same linearization of the generalized forces (Equation

2) proposed by Baraff and Witkin to obtain a semi-implicit form of the BDF2 integrator. As with Baraff and Witkin's study, the researchers do not validate the method, however they note that time-steps as large as 0.2s can be used to produce visually "believable" animations.

Only a small number of researchers have applied a semi-implicit integration method to an ANCF cable model. Sugiyama and Shabana [23] implement two methods, the Rosenbrock method and a method based on the semi-implicit midpoint rule. Both methods utilize linearizations similar to Baraff and Witkin's method. The researchers use an adaptive time-stepping scheme to control the simulation error and compare the two integrators to both explicit and implicit integration schemes for a variety of benchmark scenarios. There is limited discussion, however, of the computational performance of the methods and the use of adaptive time-stepping makes their applicability to real-time simulations unclear.

Hewlett et al. [24] develop an ANCF cable model utilizing a semi-implicit formulation developed by Servin et al. [25]. The elastic forces and external contact forces are defined as quadratic potentials representing a flexible constraint. The semi-implicit integrator simultaneously updates the nodal velocities while solving for the magnitude of the constraint forces. While Hewlett et al. account for applied forces that are not generated by a quadratic potential, only gravitational forces which are constant throughout the simulation are considered in their study. The method also demonstrates significant numerical damping. Despite these limitations Hewlett et al. produced faster than real-time simulations of flexible pendulums. However, there is no discussion of the accuracy of the proposed method relative to the fully implicit integrator and it is uncertain whether their method could be applied to ALE-ANCF elements.

1.2. Paper Summary

The principal objective of the paper is to develop a framework for applying semi-implicit numerical integration to ANCF and ALE-ANCF cable models. The proposed method comprises a generalization of Baraff and Witkin's semi-

implicit algorithm which can be applied with a variety of implicit methods. Additionally, the method addresses two challenges specific to the integration of ANCF and ALE-ANCF cable models. Firstly, an Implicit-Explicit (IMEX) scheme is proposed to handle complex or non-differentiable generalized forces. Second, the method incorporates rigid holonomic constraints, which are necessary to ensure a unique solution can be obtained for the ALE-ANCF dynamic equations.

The work also examines the utility of semi-implicit numerical integration techniques for simulating cables by comparing the accuracy and computational performance of various semi-implicit methods derived using the proposed framework to a popular full-implicit algorithm. Four benchmark studies compare the semi-implicit methods to a fully implicit Newmark solver for a variety of conditions and external forces. Unlike previous studies, the relationship between the accuracy and computation time of each method is examined to evaluate their suitability for real-time applications.

In Section 2, the ALE-ANCF cable model is described. The proposed numerical integration method is presented in Section 3. Section 4 discusses the implementation of the model and includes the results of four benchmark problems. Concluding remarks and recommendations for future work are given in Section 5.

2. ALE-ANCF Cable Model

Figure 1 illustrates the ALE-ANCF element in its initial undeformed state and in a deformed configuration. Each element consists of two nodes, each with seven degrees of freedom including the position of the in the absolute coordinate frame $\mathbf{r}$, a slope vector tangent to the centerline of the cable $\mathbf{r}'$ and a material coordinate p. The material coordinate represents the position of a point on the element, measured along the length of the unstretched cable from a reference or head point. The head point is shown in the figure as an open circle.

The vector of generalized coordinates for the element is

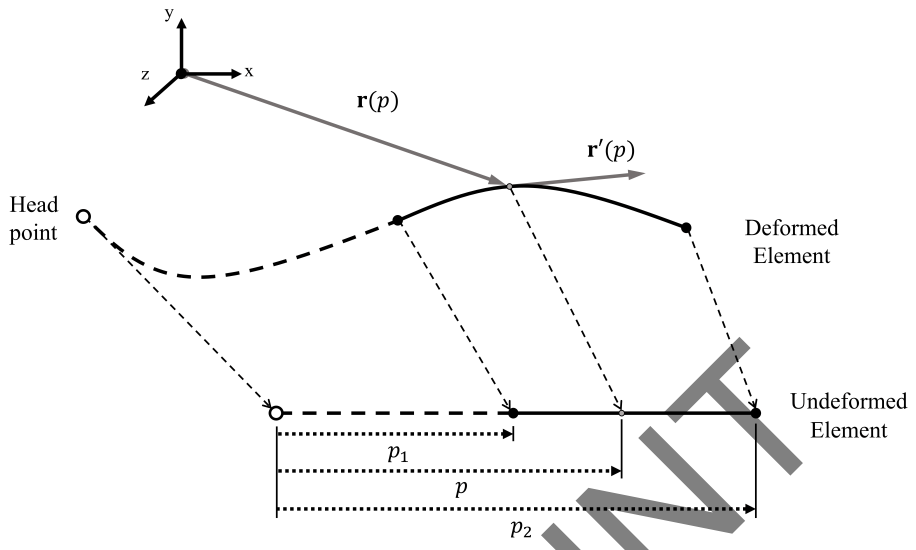

Figure 1: Deformed ALE-ANCF cable element and equivalent undeformed element in the absolute coordinate frame.

$$\mathbf{q} = [\mathbf{r}_1^T \quad (\mathbf{r}_1')^T \quad p_1 \quad \mathbf{r}_2^T \quad (\mathbf{r}_1')^T \quad p_2]^T \tag{4}$$

A second vector consisting only of the mesh coordinates is defined

$$\mathbf{q}_e = [\mathbf{r}_1^T \quad (\mathbf{r}_1')^T \quad \mathbf{r}_2^T \quad (\mathbf{r}_1')^T]^T. \tag{5}$$

The Euclidean position of a point on the element can be found by interpolating between the element nodes

$$\mathbf{r}(p) = \mathbf{S}_e \mathbf{q}_e, \tag{6}$$

where $\mathbf{S}_e$ is a cubic shape function given by

$$\mathbf{S}_e = [S_1\mathbf{I}_3 \quad S_2\mathbf{I}_3 \quad S_3\mathbf{I}_3 \quad S_4\mathbf{I}_3], \tag{7}$$

and

$$S_1 = \frac{(p-p_2)^2(2p-3p_1+p_2)}{(p_2-p_1)^3}, \tag{8a}$$

$$S_2 = \frac{(p-p_1)(p-p_2)^2}{(p_1-p_2)^2}, \tag{8b}$$

$$S_3 = \frac{(p-p_1)^2(2p+p_1-3p_2)}{(p_1-p_2)^3}, \tag{8c}$$

$$S_4 = \frac{(p-p_2)(p-p_1)^2}{(p_1-p_2)^2}. \tag{8d}$$

The unstretched length of the element l_e is given by the difference of the material coordinates at the two nodes:

$$l_e = p_2 - p_1. \tag{9}$$

Additionally, the velocity of a point on the cable is

$$\dot{\mathbf{r}} = \mathbf{S}_e\dot{\mathbf{q}}_e + \left(\frac{\partial \mathbf{S}_e}{\partial p_1}\dot{p}_1 + \frac{\partial \mathbf{S}_e}{\partial p_2}\dot{p}_2\right)\mathbf{q}_e = \mathbf{S}\dot{\mathbf{q}}, \tag{10}$$

where the shape function $\mathbf{S}$ is

$$\mathbf{S} = [S_1\mathbf{I}_3 \quad S_2\mathbf{I}_3 \quad \tfrac{\partial \mathbf{S}_e}{\partial p_1}\mathbf{q}_e \quad S_3\mathbf{I}_3 \quad S_4\mathbf{I}_3 \quad \tfrac{\partial \mathbf{S}_e}{\partial p_2}\mathbf{q}_e]. \tag{11}$$

The governing equations proposed by Hong et al. [13] are

$$\mathbf{M}\ddot{\mathbf{q}} + \mathbf{Q}_p + \mathbf{Q}_e + \mathbf{Q}_f + {\mathbf{C}_\mathbf{q}}^T\lambda = 0 \tag{12a}$$

$$\mathbf{C}(\mathbf{q}, t) = 0 \tag{12b}$$

where $\mathbf{M}$ is the element mass matrix, $\mathbf{Q}_p$ is a generalized force representing the inertial force of the cable due to changes in the material coordinates p_1 and p_2, $\mathbf{Q}_e$ is a generalized force representing the internal elastic potential, $\mathbf{Q}_f$ represents the externally applied forces and $\mathbf{C}$ represents a set of holonomic constraints. The force required to satisfy the constrains are given by the product of the constraint Jacobian ${\mathbf{C}_\mathbf{q}}^T$ and a vector of Lagrange multipliers λ.

The element mass matrix $\mathbf{M}$ is given by

$$\mathbf{M} = \int_{p_1}^{p_2} \rho A \mathbf{S}^T\ddot{\mathbf{r}}_p \mathrm{d}p, \tag{13}$$

where ρ is the cable density and A is the cross-sectional area. The additional intertia force $\mathbf{Q}_p$ is

$$\mathbf{Q}_p = \int_{p_1}^{p_2} \rho A \mathbf{S}^T \mathbf{S} \mathrm{d}p. \tag{14}$$

The generalized elastic forces are

$$\mathbf{Q}_e = \int_{p_1}^{p_2} EA \left(\frac{\partial \varepsilon}{\partial \mathbf{q}} \right)^T \varepsilon \mathrm{d}p + \frac{1}{2} \int_{p_1}^{p_2} EI \left(\frac{\partial \kappa}{\partial \mathbf{q}} \right)^T \kappa \mathrm{d}p, \tag{15}$$

where ε is the longitudinal strain, κ is the element curvature and E is the elastic modulus of the cable. In the current study the strain and curvature follow the authors' previous work [8] and are defined as

$$\varepsilon = (\mathbf{r}_p^T \mathbf{r}_p - 1), \tag{16}$$

$$\kappa = |\mathbf{r}_{pp}|. \tag{17}$$

Finally, external distributed forces $\mathbf{f}(p)$ have a corresponding generalized force calculated as

$$\mathbf{Q}_f = -\int_{p_1}^{p_2} \mathbf{S}^T \mathbf{f} \mathrm{d}p. \tag{18}$$

The kinematic constraints represented by the constraint matrix $\mathbf{C}$ can be used to implement boundary conditions, such as pin joints, or to constrain the material coordinates of the element. If the material coordinates p_1 and p_2 of the element are held fixed, the ALE-ANCF method is equivalent to the traditional gradient-deficient ANCF method proposed by Shabana [6]. Additionally, the ALE-ANCF mass matrix given by Equation 13 is rank-deficient. Constraints must therefore be carefully selected such that the equations of motion (Equations 12a and b) have a unique solution. Since a force acting axially along the cable could effect motion of the finite element mesh or the cable material moving independent of the mesh, either the mesh coordinates $\mathbf{r}$ or the material coordinates p must be constrained to eliminate the redundancy. The application of these constraints is discussed further in the following section along with the numerical integration method.

3. Proposed Integration Method

A general method is proposed which can be used to apply a semi-implicit form of an implicit ODE solver to solve multibody dynamics problems including ANCF and ALE-ANCF models. While the method can be derived for a variety of implicit integrators, the derivation of the proposed semi-implicit integrator using the Newmark method is shown below.

The Newmark method is described by two equations for updating the generalized coordinates and their velocities from time-step n to time-step $n+1$:

$$\mathbf{v}_{n+1} = \mathbf{v}_n + (1-\gamma)h\mathbf{a}_n + \gamma h\mathbf{a}_{n+1} \tag{19a}$$

$$\mathbf{q}_{n+1} = \mathbf{q}_n + h\mathbf{v}_n + \frac{h^2}{2}[(1-2\beta)\mathbf{a}_n + 2\beta\mathbf{a}_{n+1}] \tag{19b}$$

where γ and β are parameters which define the variation of acceleration over the time-step ($\gamma = 0.5$ and $\beta = 0.25$ represent the commonly used trapezoidal rule).

For a multibody system with holonomic constraints, the generalized equations of motion are defined as a set of Differential Algebraic Equations (DAEs) given by

$$\mathbf{Ma} - \mathbf{C_q}^T\lambda = \mathbf{Q} \tag{20a}$$

$$\mathbf{C}(\mathbf{q}, t) = 0 \tag{20b}$$

where $\mathbf{C}$ is an vector of constraint equations, $\mathbf{C_q}$ is the Jacobian matrix of the constraint equations with respect to the generalized coordinates $\mathbf{q}$, and λ is a vector of Lagrange multipliers representing the magnitude of the constraint force.

Taking Equation 19a at time-step $n+1$ and applying the Taylor series expansion proposed by Baraff and Witkin we obtain

$$\mathbf{M}\mathbf{a}_{n+1} + \mathbf{C_q}^T\lambda_{n+1} = \mathbf{Q}_n + \mathbf{J_q}(\mathbf{q}_{n+1} - \mathbf{q}_n) + \mathbf{J_v}(\mathbf{v}_{n+1} - \mathbf{v}_n) \tag{21}$$

where $\mathbf{J_q} = \partial\mathbf{Q}/\partial\mathbf{q}$ and $\mathbf{J_v} = \partial\mathbf{Q}/\partial\mathbf{v}$. The mass matrix $\mathbf{M}$ is assumed to be constant. Substituting Equations 19a and b and grouping the terms containing $\mathbf{a}_{n+1}$:

$$\left(\mathbf{M} - h^2\beta\mathbf{J_q} - \gamma h\mathbf{J_v}\right)\mathbf{a}_{n+1} + \mathbf{C_q}^T\lambda_{n+1} = \mathbf{Q}_n + \mathbf{J_v}(1-\gamma)h\mathbf{a}_n + \mathbf{J_q}\left[h\mathbf{v}_n + \frac{h^2}{2}(1-2\beta)\mathbf{a}_n\right] \tag{22}$$

To ensure that the constraint Jacobian $\mathbf{C_q}$ has a known at time-step $n+1$, the constraint equations $\mathbf{C}$ are restricted to those of the form

$$\mathbf{C}(\mathbf{q}, t) = \mathbf{A}^T\mathbf{q} - \mathbf{b}(t) = 0 \tag{23}$$

where $\mathbf{A}$ is a constant matrix and $\mathbf{b}$ is a known function of time. To mitigate drift of the constraint due to numerical error, constraint stabilization [26] is applied by replacing Equation 20b with

$$\ddot{\mathbf{C}} + 2a_1\dot{\mathbf{C}} + a_2^2\mathbf{C} = 0 \tag{24}$$

where a_1 and a_2 are chosen constants. The constraint is thus enforced at the acceleration level with proportional and derivative feedback terms to compensate for any accumulated error.

Combining Equations 22–24, the following linear system of equations is obtained:

$$\begin{bmatrix} \mathbf{H}_n & \mathbf{A}^T \\ \mathbf{A} & \mathbf{0} \end{bmatrix}\begin{bmatrix} \mathbf{a}_{n+1} \\ \lambda_{n+1} \end{bmatrix} = \begin{bmatrix} \mathbf{R}_n \\ \ddot{\mathbf{b}}_{n+1} - 2a_1\dot{\mathbf{C}}_n - a_2^2\mathbf{C}_n \end{bmatrix} \tag{25}$$

where, at time-step n, $\mathbf{H}_n$ and $\mathbf{R}_n$ are defined for convenience as

$$\mathbf{H}_n = \mathbf{M}_n - h^2\beta\mathbf{J}_{\mathbf{q},n} - \gamma h\mathbf{J}_{\mathbf{v},n} \tag{26a}$$

$$\mathbf{R}_n = \mathbf{Q}_n + \mathbf{J}_{\mathbf{v},n}(1-\gamma)h\mathbf{a}_n + \mathbf{J}_{\mathbf{q},n}\left[h\mathbf{v}_n + \frac{h^2}{2}(1-2\beta)\mathbf{a}_n\right]. \tag{26b}$$

Note that the second and third terms of Equation 24 are calculated using the system states at time-step n, since their values at the forthcoming time-step are unknown. Equation 25 can be solved for $\mathbf{a}_{n+1}$ and λ_{n+1} using a common linear solver such as MATLAB's *linsolve*. Finally, $\mathbf{a}_{n+1}$ can be substituted into the time-stepping equations (Equations 19a and b) to determine the generalized coordinates and velocities at time-step $n+1$.

The proposed integrator, represented by Equation 25, can be formulated based on a variety of implicit solvers. In this study, the Backward Euler, BDF2 and Hilber-Hughes-Taylor (HHT) methods are considered in addition to the Newmark method shown above. For the HHT method, the equations of motion utilized by Negrut et al. [27] are used in place of Equation 20a, and are given by

$$\mathbf{M}\mathbf{a}_{n+1} + \alpha(\mathbf{C_q}^T\lambda - \mathbf{Q})_n + (1-\alpha)(\mathbf{C_q}^T\lambda - \mathbf{Q})_{n+1} = 0 \tag{27}$$

where α is a free parameter to adjust the numerical damping. If an α value of 0 is selected, the method is identical to the Newmark method. Table 1 summarizes the equations derived for each of the four methods. In the remainder of this paper, the four methods in their Semi-Implicit (SI) forms are notated as SI Backward Euler, SI BDF2, SI Newmark and SI HHT.

In some cases where the generalized forces are complex or are not continuously differentiable, the Jacobian matrices $\mathbf{J_q}$ and $\mathbf{J_v}$ may be difficult to calculate analytically. A common approach used in other semi-implicit schemes is to partition the generalized forces into "stiff" and "non-stiff" components, $\mathbf{Q}_S$ and $\mathbf{Q}_{NS}$, respectively. The non-stiff forces are then treated as if they are constant throughout the time-step and are thus handled explicitly by the integrator. This partitioning of the forces is referred to as an Implicit-Explicit (IMEX) method. The Taylor series expansion of the generalized forces becomes

$$\begin{aligned}\mathbf{Q}_{n+1} &= \mathbf{Q}_{S,n+1} + \mathbf{Q}_{NS,n+1} \\ &\approx \mathbf{Q}_{S,n} + \frac{\partial \mathbf{Q}_S}{\partial \mathbf{q}}\Delta\mathbf{q} + \frac{\partial \mathbf{Q}_S}{\partial \mathbf{v}}\Delta\mathbf{v} + \mathbf{Q}_{NS,n}\end{aligned} \tag{28}$$

Table 1: Summary of equations for semi-implicit integration methods

Method	Time-Stepping Equations	$\mathbf{H}_n$	$\mathbf{R}_n$
Backward Euler	$\mathbf{q}_{n+1} = \mathbf{q}_n + h\mathbf{v}_{n+1}$ $\mathbf{v}_{n+1} = \mathbf{v}_n + h\mathbf{a}_{n+1}$	$\mathbf{M}_n - h^2\mathbf{J}_{\mathbf{q},n} - h\mathbf{J}_{\mathbf{v},n}$	$\mathbf{Q}_n + h\mathbf{J}_{\mathbf{q},n}\mathbf{v}_n$
BDF2	$\mathbf{q}_{n+1} = \frac{4}{3}\mathbf{q}_n - \frac{1}{3}\mathbf{q}_{n-1} + \frac{2}{3}h\mathbf{v}_{n+1}$ $\mathbf{v}_{n+1} = \frac{4}{3}\mathbf{v}_n - \frac{1}{3}\mathbf{v}_{n-1} + \frac{2}{3}h\mathbf{a}_{n+1}$	$\mathbf{M}_n - \frac{4}{9}h^2\mathbf{J}_{\mathbf{q},n} - \frac{2}{3}h\mathbf{J}_{\mathbf{v},n}$	$\mathbf{Q}_n + \mathbf{J}_{\mathbf{q},n}(\frac{8}{9}h\mathbf{v}_n - \frac{2}{9}h\mathbf{v}_{n-1} + \frac{1}{3}\mathbf{q}_n - \frac{1}{3}\mathbf{q}_{n-1}) + \mathbf{J}_{v,n}(\frac{1}{3}\mathbf{v}_n - \frac{1}{3}\mathbf{v}_{n-1})$
Newmark	$\mathbf{q}_{n+1} = \mathbf{q}_n + h\mathbf{v}_n + \frac{1}{2}h^2[(1-2\beta)\mathbf{a}_n + 2\beta\mathbf{a}_{n+1}]$ $\mathbf{v}_{n+1} = \mathbf{v}_n + h(1-\gamma)\mathbf{a}_n + h\gamma\mathbf{a}_{n+1}$	$\mathbf{M}_n - h^2\beta\mathbf{J}_{\mathbf{q},n} - h\gamma\mathbf{J}_{\mathbf{v},n}$	$\mathbf{Q}_n + \mathbf{J}_{\mathbf{q},n}[h\mathbf{v}_n + \frac{1}{2}h^2(1-2\beta)\mathbf{a}_n] + \mathbf{J}_{\mathbf{v},n}(1-\gamma)h\mathbf{a}_n$
HHT	Same as Newmark	$\frac{1}{1+\alpha}\mathbf{M}_n - h^2\beta\mathbf{J}_{\mathbf{q},n} - h\gamma\mathbf{J}_{\mathbf{v},n}$	$\frac{\alpha}{1+\alpha}(\mathbf{A}^T\lambda_n - \mathbf{Q}_n) + \mathbf{Q}_n + \mathbf{J}_{\mathbf{q},n}[h\mathbf{v}_n + \frac{1}{2}h^2(1-2\beta)\mathbf{a}_n] + \mathbf{J}_{\mathbf{v},n}(1-\gamma)h\mathbf{a}_n$

Since the non-stiff forces are held constant, they do not contribute to the Jacobian matrices. In the present study, the internal elastic and inertial forces are considered stiff. External forces which are purely dissipative, such as hydrodynamic and friction forces, are considered non-stiff.

4. Simulations and Results

Three benchmark cases are considered in this section. The first consists of a flexible tether pinned at one end and released from a horizontal position. The second benchmark study consists of a flexible tether submerged in water. In both cases, all material coordinates are fixed, reducing the model to the traditional ANCF method. In the final case the ALE-ANCF method is utilized to simulate a flexible cable sliding over the edge of a table. The second and third cases demonstrate the IMEX integration method, as the hydrodynamic and surface friction forces are handled explicitly.

For each benchmark, the proposed semi-implicit methods are compared against the fully implicit Newmark method, chosen for its high accuracy and minimal numerical damping. The implementation of the Newmark method is taken from Negrut et al.'s implementation of the HHT method [27] with no added numerical damping, i.e. an α value of zero. Negrut et al. propose an adaptive time-stepping algorithm, where the time-step varies to keep the simulation error below a user specified tolerance. In this work an absolute error tolerance of 1×10^{-6} is selected. Full details of the fully implicit algorithm can be found in Negrut et al.'s paper [27].

The ALE-ANCF model was coded in MATLAB where the generalized elastic forces $\mathbf{Q}_e$ and inertial forces $\mathbf{Q}_p$ were derived using MATLAB's symbolic toolbox. The Jacobian matrices for each force were then determined using symbolic differentiation. The symbolic functions are then converted to MATLAB functions to be called during the simulation. All simulations were performed on an Intel Core i7-6700 processor with 16GB of RAM.

For each test, the cable considered has a diameter of 1 cm, a linear density

of 5000 kg/m and a moment of inertia of 1×10^{-8} m^4. Various values of the elastic modulus E are considered to examine the model under varying levels of stiffness. With a bending stiffness EI of approximately 1 Nm^2 ($E = 1 \times 10^8$ Pa), the cable is expected to behave similar to a steel wire rope. In each case, the cable is composed of ten ALE-ANCF elements.

4.1. Benchmark 1: Flexible Pendulum

The first benchmark study consists of an unloaded flexible cable pinned at one end which is released from an initial horizontal position and allowed to swing. The cable has a length of 1 m. Three values of the elastic modulus E were considered (1×10^7, 1×10^8 and 1×10^9 Pa) in order to evaluate the accuracy and performance of the proposed methods for various levels of stiffness. For each of the four integration methods chosen, the cable motion was simulated using various time-steps ranging from 1×10^{-4} to 1×10^{-2} s for a total simulation time of 10 s. Additionally, the simulations were performed with the fully implicit Newmark method with adaptive time-stepping.

Figure 2a shows the cable profile at various points in time for the simulation with $E = 1 \times 10^7$ and $E = 1 \times 10^9$ Pa. For the former case, the cable behaves like a flexible rope or tether due to the low stiffness. With a higher stiffness, the cable behaves closer to a rigid rod, with limited transverse deformation.

For each of the semi-implicit integration methods, the computation times of the simulations are approximately equal. Table 2 presents the computation times for the fully implicit and semi-implicit Newmark methods. For the fully-implicit Newmark, the computation time varies significantly depending on the cable stiffness, ranging from 89 to 566 s for 10 s of simulated motion. For the proposed SI Newmark method, the computation times are shown for each of the time-steps considered. Real-time simulations are obtained for time-steps of 2.5×10^{-3} s or greater. For all time-steps greater than or equal to 2.5×10^{-4} the computations times were smaller using the proposed method compared to the fully-implicit Newmark.

The Mean Absolute Error (MAE) of the vertical position the cable tip was

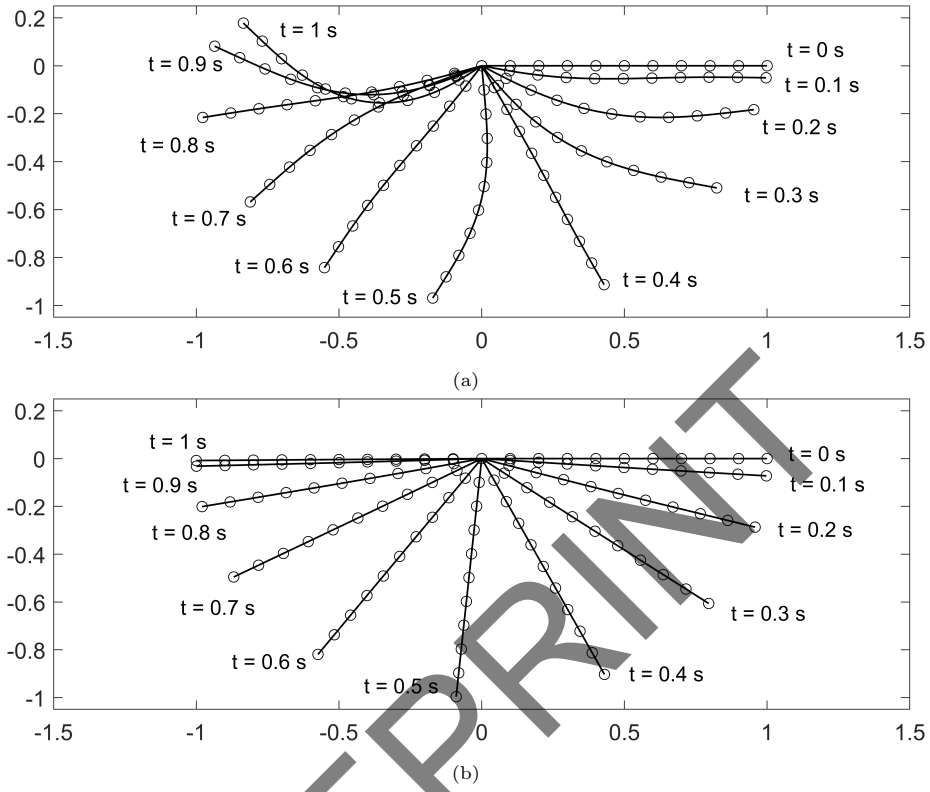

Figure 2: Flexible pendulum motion simulated using the implicit Newmark method with (a) $E = 1 \times 10^7$ Pa and (b) $E = 1 \times 10^9$ Pa. Element nodes are shown as open circles.

calculated for each simulation relative to the results obtained using the fully-implicit method. Tables 3, 4 and 5 present the results for the three elastic moduli considered. In all three cases, the SI BE method demonstrated the largest error of the four methods. The errors for the SI Nemark, SI HHT, and SI BDF2 were comparable for each of the three cases. However, the SI Newmark demonstrated instability for three of the simulations performed. The additional damping provided by the HHT and BDF2 algorithms serves to stabilize the simulations without a significant increase in error.

In all cases, the error increased with larger time-steps due to the increase in numerical damping. This energy loss due to numerical damping likely stems from the truncation error created by the Taylor series approximation in Equation

Table 2: Computation times of flexible pendulum simulation for the proposed method and fully-implicit Newmark method. The length of each simulation was 10 s. The computation times for the fully-implicit method are reported for each of the three Elastic moduli (1×10^7 Pa, 1×10^8 Pa, and 1×10^9 Pa). Computation times for the proposed method are averages of all simulations using the SI Newmark method.

Time-step, h (s)	Computation Time (s)
Fully-implicit (adaptive)	566.3/89.1/105.3
1×10^{-4}	158.0
2.5×10^{-4}	63.0
5×10^{-4}	32.1
1×10^{-3}	15.6
2.5×10^{-3}	6.5
5×10^{-3}	3.7
1×10^{-2}	1.7

Table 3: Mean Absolute Error (MAE) in mm of proposed methods relative to the fully-implicit Newmark method for flexible pendulum simulation with $E = 1 \times 10^7$

Time step, h (s)	SI Newmark	SI HHT	SI BDF2	SI BE
1×10^{-4}	19.25	21.45	24	55.06
2.5×10^{-4}	18.63	31.38	15.65	72.26
5×10^{-4}	31.47	21.09	30.52	91.46
1×10^{-3}	*	20.23	53.76	147.84
2.5×10^{-3}	81.02	52.10	112.85	154.69
5×10^{-3}	148.94	145.74	135.31	189.42
1×10^{-2}	*	157.08	156.40	292.51

* Simulation unstable

2. Figure 3 plots the total energy of the cable as a function of time for the SI Newmark method with an elastic modulus of 1×10^8 Pa. Minimal energy loss is

Table 4: Mean Absolute Error (MAE) in mm of proposed methods relative to the fully-implicit Newmark method for flexible pendulum simulation with $E = 1 \times 10^8$

Time step, h (s)	SI Newmark	SI HHT	SI BDF2	SI BE
1×10^{-4}	0.35	0.35	0.33	24.64
2.5×10^{-4}	0.39	0.38	0.35	59.19
5×10^{-4}	0.86	0.79	0.65	110.79
1×10^{-3}	5.51	4.98	4.87	192.08
2.5×10^{-3}	76.14	69.40	73.91	312.99
5×10^{-3}	301.84	291.60	299.36	370.51
1×10^{-2}	428.64	417.92	424.03	460.45

Table 5: Mean Absolute Error (MAE) in mm of proposed methods relative to the fully-implicit Newmark method for flexible pendulum simulation with $E = 1 \times 10^9$

Time step, h (s)	SI Newmark	SI HHT	SI BDF2	SI BE
1×10^{-4}	0.065	0.061	0.075	24.47
2.5×10^{-4}	0.79	0.71	0.67	59.49
5×10^{-4}	6.23	5.63	5.90	114.32
1×10^{-3}	47.52	43.11	46.75	211.08
2.5×10^{-3}	314.78	306.36	313.93	348.15
5×10^{-3}	434.85	424.54	430.55	447.67
1×10^{-2}	*	506.05	508.43	511.75

* Simulation unstable

observed for small time-steps, however higher time-steps produce nearly critical damping of the pendulum motion. Figure 4 shows the energy loss for the four proposed integrators with a time-step of 1×10^{-3} s. The three second order methods exhibit nearly identical damping behavior, while the first order BE integrator exhibits much greater dissipation than the other methods. Thus the large errors demonstrated by the SI BE method relative to the fully-implicit

method can be explained by the increase in numerical damping.

The computation times indicate that the proposed method is suitable for real-time applications. Stable real-time simulations were obtained using all four methods, however the SI Newmark method demonstrated instability in several cases and is thus not recommended. Comparing the results obtained using the semi-implicit and fully-implicit methods, illustrates the relationship between accuracy and time-step. As the time-step increases, the amount of numerical dissipation increases, attenuating the pendulum motion. It is therefore important to use the smallest time-step possible in order to maintain the accuracy of the simulation. In systems with significant physical damping, such as submerged cables or systems with surface friction, the impact of the numerical damping may be lessened. The following two benchmark studies will examine these types of systems. Since the SI HHT method demonstrated the smallest errors overall for the flexible pendulum case, it will be used in the two remaining benchmark studies.

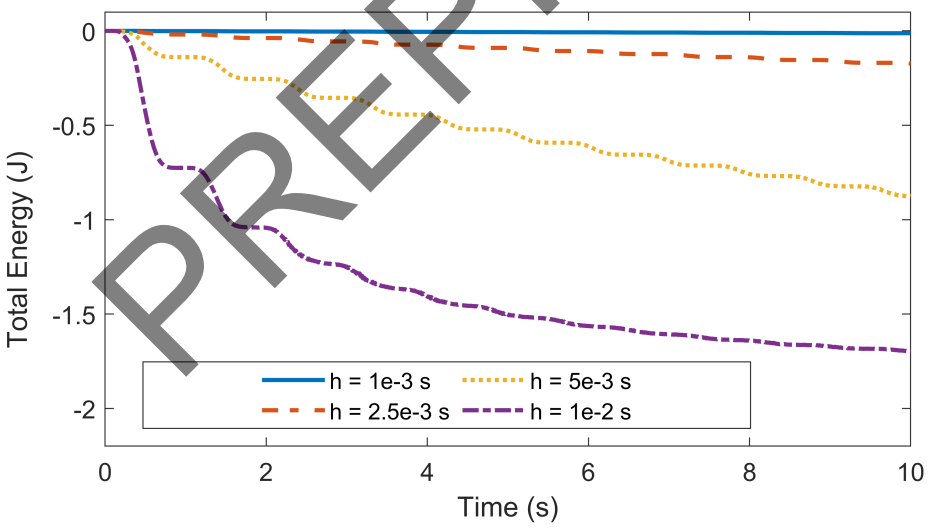

Figure 3: Total energy of flexible pendulum as a function of time for the SI Newmark method.

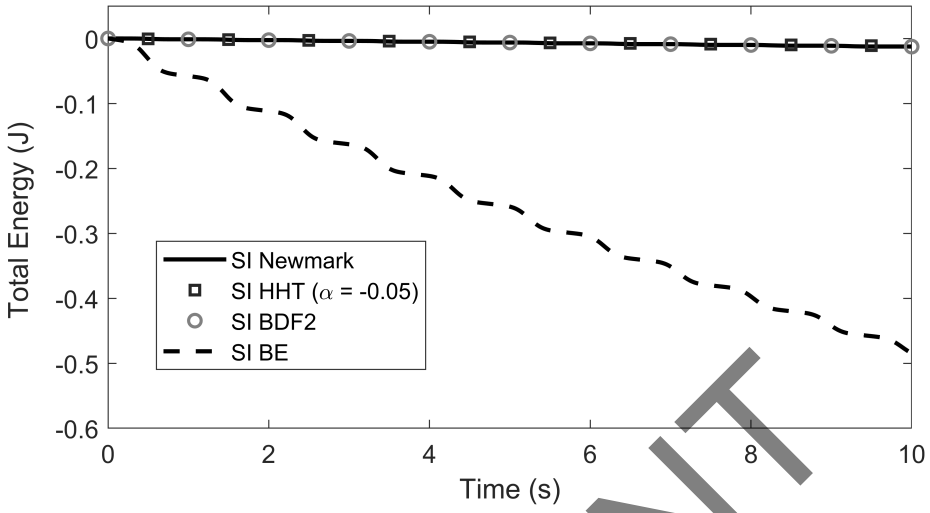

Figure 4: Total energy of flexible pendulum as a function of time for the four semi-implicit methods with $h = 1 \times 10^{-3}$ s and $E = 1 \times 10^{8}$ Pa.

4.2. Benchmark 2: Submerged Tether

The second benchmark is inspired by the physical experiments performed by Takehara et al. [28] to validate their ANCF cable model. The simulation consists of a cable or tether with an elastic modulus $E = 1 \times 10^{8}$ Pa submerged in water and pinned at one end. Two scenarios are considered and illustrated in Figure 5. First, the cable is initially horizontal and released. In the second case, the cable is initially horizontal with a linear motion applied to the pin connection.

The external forces applied to the cable include gravitational and hydrodynamic drag and added mass forces. These forces are treated as non-stiff, since they are purely dissipative. The generalized external force shown in Equation 18 is approximated using a five-point Gaussian quadrature. A detailed description of the hydrodynamic force model is given in [8].

For the first test case, 2.5 s of motion is simulated. Figure 6 shows the vertical motion of the cable tip for the fully-implicit Newmark and SI HHT methods. In the second case, the base of the tether is translated at a constant velocity of 0.5 m/s for 2 seconds and then brought to rest. A total of 10 s of

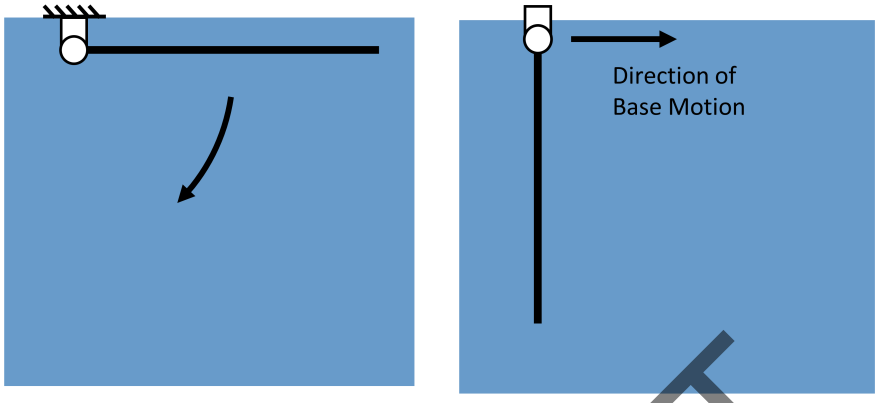

(a) (b)

Figure 5: Illustrations of the submerged pendulum for (a) Case 1 and (b) Case 2.

motion was simulated. Figure 7 compares the horizontal position of the cable tip for the two integrators.

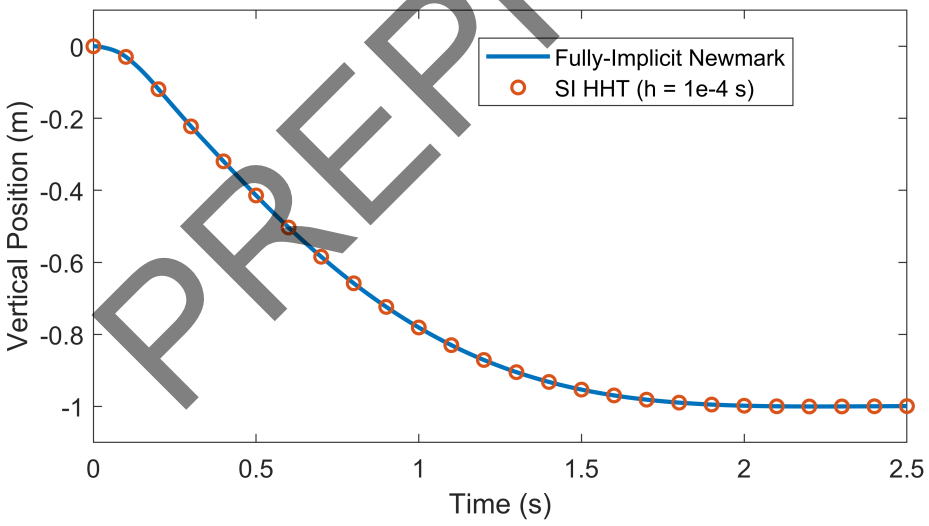

Figure 6: Simulated vertical position of the cable tip for submerged tether (Case 1).

Simulations were again performed using the SI HHT method with a range of time-steps. The computation time and error for each simulation is presented in Table 6. The error between the fully and semi-implicit simulations is calculated

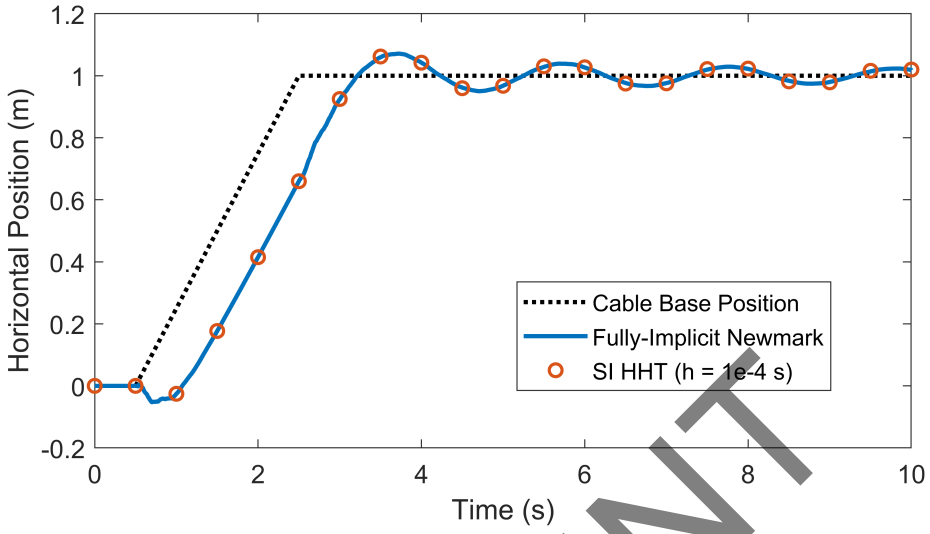

Figure 7: Simulated horizontal position of the cable tip and base for submerged tether (Case 2).

based on the Euclidean position of the cable tip. For both test cases, the semi-implicit HHT method demonstrated significantly higher computation speeds, with minimal error. For Case 1, the MAE for a time-step of 1×10^{-2} s was 2.58 mm or 0.26% of the full range of motion and a 770 times improvement in computation time was obtained over the fully-implicit method. Similar results were obtained for Case 2, with a maximum error of 9.62 mm or 0.96% of the full range of motion with computation times as low as 6.5 s compared to 3453 s for the fully-implicit method. As expected, in the presence of significant external damping the numerical damping has less of an effect on the simulation accuracy as the time-step increases. Faster-than-real-time simulations were obtained with errors of only 1% of the full range of motion, indicating the proposed method is suitable for applications involving submerged cables.

4.3. Benchmark 3: Sliding Tether

The final case study consists of a flexible cable partially resting on a flat surface with a second segment hanging vertically. Figure 8 illustrates the system. The finite element nodes are shown as closed circles. The open circle

Table 6: Computation times and Mean Absolute Error of the proposed method compared to the fully-implicit Newmark method for the submerged tether system. Errors are calculated as the Euclidean distance of the cable tip between the two simulations. The total simulation time was 2.5 s for Case 1 and 10 s for Case 2.

	Case 1		Case 2	
Time-step, h (s)	Time (s)	MAE (mm)	Time (s)	MAE (mm))
Fully-implicit (adaptive)	1242.4	–	3453.0	–
1×10^{-4}	173.4	0.028	640.0	1.27
2.5×10^{-4}	71.5	0.071	266.8	1.20
5×10^{-4}	30.6	0.14	145.9	0.88
1×10^{-3}	15.2	0.28	64.2	1.74
2.5×10^{-3}	6.2	0.69	25.7	2.16
5×10^{-3}	3.1	1.36	13.0	7.46
1×10^{-2}	1.6	2.58	6.5	9.62

represents a transition node, which is fixed in space. The material coordinate p_1 corresponding to the transition node is unconstrained allowing material to flow between the adjacent elements. This flow of material emulates the cable sliding over the edge of the surface, without the need to model the curvature of the cable at the transition. The simulations start with 0.5 m of cable resting on the surface and 0.5 m of cable hanging vertically.

Since the tether is assumed to bend over the edge of the surface with zero radius of curvature, a small bending stiffness of 0.1 Nm^2 ($E = 1 \times 10^7$ Pa) is used to make this assumption realistic. On the vertical cable segment, gravitational forces are applied. On the segment in contact with the surface, a tangential friction force is applied. The friction force per unit length is calculated as

$$\mathbf{f} = \begin{cases} -\mu\rho g \,\mathrm{sgn}(v), & |v| > \epsilon \\ -\mu\rho g v/\epsilon, & |v| \leq \epsilon \end{cases} \tag{29}$$

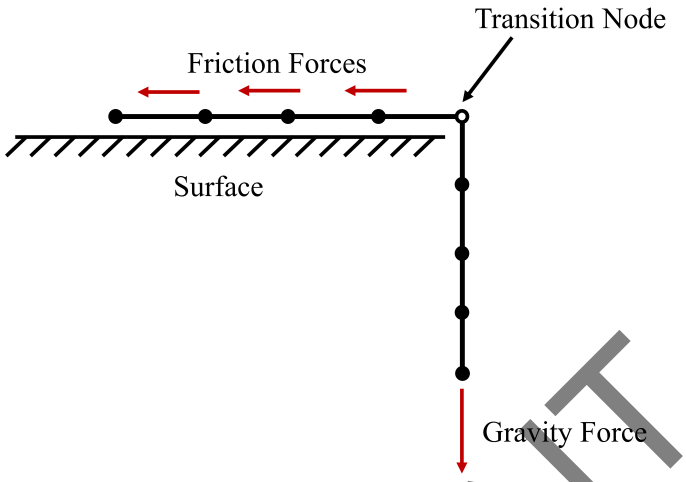

Figure 8: Illustration of sliding tether system.

where v is the sliding velocity, μ is a friction coefficient, and ϵ is a regularization parameter. The friction force is treated as non-stiff for the purpose of calculating the force Jacobians. Simulations are performed both without friction and with a friction coefficient of $\mu = 0.4$. The regularization parameter ϵ is selected to be 0.001 m/s.

Figure 9 shows the simulated tether displacement as a function of time for the fully-implicit Newmark and SI HHT methods. For the simulations without friction, 0.4 s of motion was simulation, whereas 0.8 s of motion was simulated with friction. The computation time and MAEs of the SI method compared to the fully-implicit Newmark are shown in Table 7. For the case without friction the error remains relatively constant regardless of the time-step and are within 1% of the full range of motion for every time-step considered. For the case with friction, the errors are small for time-steps of 1×10^{-3} s or smaller but increase as a result of numerical damping for larger time-steps. Real-time simulations are obtained with errors of 13.3 mm (5.5% of the full range of motion) for time-steps of 1×10^{-2} s as the numerical dissipation increases.

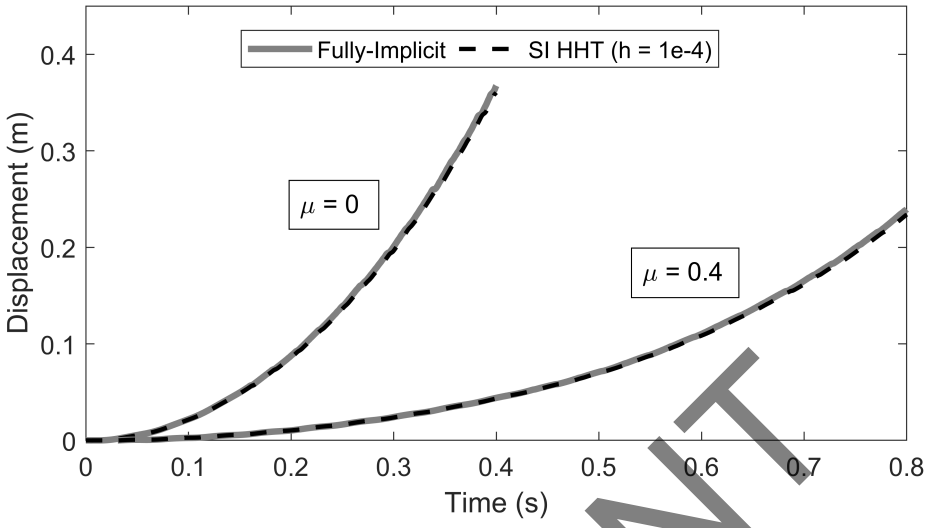

Figure 9: Cable displacement as a function of time for sliding tether simulation.

Table 7: Computation times and Mean Absolute Error of the proposed method and fully-implicit Newmark method for sliding tether system. Errors are calculated based on the displacement of the first cable node. The total simulation time was 0.4 s for Case 1 and 0.8 s for Case 2.

	Case 1 ($\mu = 0$)		Case 2 ($\mu = 0.4$)	
Time-step, h (s)	Time (s)	MAE (mm)	Time (s)	MAE (mm))
Fully-implicit (adaptive)	931.14	–	1251.70	–
1×10^{-4}	17.23	2.30	35.53	1.20
2.5×10^{-4}	7.35	2.34	13.66	0.82
5×10^{-4}	3.47	2.39	7.21	0.65
1×10^{-3}	1.80	2.52	3.38	3.03
2.5×10^{-3}	0.79	2.57	1.47	10.11
5×10^{-3}	0.39	2.16	0.76	13.28
1×10^{-2}	0.23	3.83	0.40	27.89

5. Conclusion

In this paper, a framework for integrating the equations of motion of ANCF and ALE-ANCF cable models using semi-implicit methods is presented. Four semi-implicit methods are derived from popular implicit integration methods. Finally, the proposed methods were compared against the fully implicit Newmark method for a variety of benchmark tests.

For the first test, a falling pendulum was simulated using the four semi-implicit methods and compared to the fully-implicit Newmark. For time-steps of 2.5×10^{-4} s or greater, the proposed semi-implicit method was faster than the fully-implicit method. In general, the SI HHT, SI BDF2 and SI Newmark exhibited similar amounts of error, however the SI Newmark method demonstrated instability in several cases. For all methods, the error increased with the time-step as a result of increased numerical damping, thus the time-step should be minimized to reduce the amount of dissipation. The SI BE method demonstrated significantly higher dissipation than the other methods considered, and thus demonstrated the highest errors. The variation in error was also examined as a function of the elastic modulus of the cable.

The final two benchmark studies incorporated more complex external forces. In Benchmark 2, a submerged pendulum was considered. In Benchmark 3, a tether sliding over the edge of a surface was simulated using the ALE-ANCF method. The SI HHT method was compared against the fully-implicit integrator. In both cases, the SI HHT demonstrated only small errors and significant improvements in computation times over the Newmark method.

The results demonstrate that the proposed semi-implicit method is a viable strategy for real-time simulations of ANCF and ALE-ANCF cable models. While the utility of the method is impacted by the numerical dissipation which limits the accuracy of the simulations for large time-steps, the computation times demonstrated in the current study were obtained using a preliminary implementation of the method in MATLAB. To improve the speed of the simulations, a compiled programming language and parallel processing may be utilized,

allowing for more accurate real-time applications. Future work will also examine other types of implicit integrators using the framework given in this paper, which may exhibit reduced numerical damping. Alternative methods which may be examined include higher order integrators such as the Runge-Kutta methods and multi-step methods such as Adams-Moulton methods. Ultimately, the amount of error which is acceptable for a given simulation depends on the use case. The model and the chosen integrator should be validated using physical experiments in order to quantify the accuracy of the combined method.

Acknowledgments

The authors acknowledge the support of the Natural Sciences and Engineering Research Council of Canada (NSERC), reference number RGPIN-2017-06967, and the Ontario Graduate Scholarship (OGS).

References

[1] T. Moi, A. Cibicik, T. Rølvåg, Digital twin based condition monitoring of a knuckle boom crane: An experimental study, Engineering Failure Analysis 112 (2020) 104517. doi:https://doi.org/10.1016/j.engfailanal.2020.104517.

[2] C. Ablow, S. Schechter, Numerical simulation of undersea cable dynamics, Ocean engineering 10 (6) (1983) 443–457. doi:https://doi.org/10.1016/0029-8018(83)90046-X.

[3] J. Gobat, M. Grosenbaugh, Application of the generalized-α method to the time integration of the cable dynamics equations, Computer Methods in Applied Mechanics and Engineering 190 (37-38) (2001) 4817–4829.

[4] J. Winget, R. Huston, Cable dynamics—a finite segment approach, Computers & Structures 6 (6) (1976) 475–480. doi:https://doi.org/10.1016/0045-7949(76)90042-0.

[5] B. Buckham, F. R. Driscoll, M. Nahon, Development of a finite element cable model for use in low-tension dynamics simulation, J. Appl. Mech. 71 (4) (2004) 476–485. doi:https://doi.org/10.1115/1.1755691.

[6] A. A. Shabana, Flexible multibody dynamics: review of past and recent developments, Multibody system dynamics 1 (2) (1997) 189–222. doi:https://doi.org/10.1023/A:1009773505418.

[7] C. Westin, Modelling and simulation of marine cables with dynamic winch and sheave contact, Master's thesis, Carleton University (2018). doi:https://doi.org/10.22215/etd/2018-13246.

[8] C. Westin, R. A. Irani, Modeling dynamic cable–sheave contact and detachment during towing operations, Marine Structures 77 (2021) 102960. doi:https://doi.org/10.1016/j.marstruc.2021.102960.

[9] U. Lugrís, J. Escalona, D. Dopico, J. Cuadrado, Efficient and accurate simulation of the rope–sheave interaction in weight-lifting machines, Proceedings of the Institution of Mechanical Engineers, Part K: Journal of Multi-body Dynamics 225 (4) (2011) 331–343. doi:https://doi.org/10.1177/1464419311403224.

[10] C. Westin, R. A. Irani, Cable-pulley interaction with dynamic wrap angle using the absolute nodal coordinate formulation, in: Proceedings of the 4th International Conference of Control, Dynamic Systems, and Robotics, 2017. doi:10.11159/cdsr17.133.

[11] R. Bulin, M. Hajžman, P. Polach, Nonlinear dynamics of a cable–pulley system using the absolute nodal coordinate formulation, Mechanics Research Communications 82 (2017) 21–28. doi:https://doi.org/10.1016/j.mechrescom.2017.01.001.

[12] F. Sheng, Z. Zhong, K.-H. Wang, Theory and model implementation for analyzing line structures subject to dynamic motions of large deformation and elongation using the absolute nodal coordinate formulation

(ancf) approach, Nonlinear Dynamics 101 (1) (2020) 333–359. doi:https://doi.org/10.1007/s11071-020-05783-4.

[13] D. Hong, J. Tang, G. Ren, Dynamic modeling of mass-flowing linear medium with large amplitude displacement and rotation, Journal of Fluids and Structures 27 (8) (2011) 1137–1148. doi:https://doi.org/10.1016/j.jfluidstructs.2011.06.006.

[14] G. Fotland, C. Haskins, T. Rølvåg, Trade study to select best alternative for cable and pulley simulation for cranes on offshore vessels, Systems Engineering 23 (2) (2020) 177–188. doi:https://doi.org/10.1002/sys.21503.

[15] J. L. Escalona, An arbitrary lagrangian–eulerian discretization method for modeling and simulation of reeving systems in multibody dynamics, Mechanism and Machine Theory 112 (2017) 1–21. doi:https://doi.org/10.1016/j.mechmachtheory.2017.01.014.

[16] J. Tang, G. Ren, W. Zhu, H. Ren, Dynamics of variable-length tethers with application to tethered satellite deployment, Communications in Nonlinear Science and Numerical Simulation 16 (8) (2011) 3411–3424. doi:https://doi.org/10.1016/j.cnsns.2010.11.026.

[17] J. Sun, Q. Tian, H. Hu, N. L. Pedersen, Topology optimization of a flexible multibody system with variable-length bodies described by ALE-ANCF, Nonlinear Dynamics 93 (2) (2018) 413–441. doi:https://doi.org/10.1007/s11071-018-4201-6.

[18] J. G. De Jalon, E. Bayo, Kinematic and dynamic simulation of multibody systems: the real-time challenge, Springer-Verlag, New York, 2012.

[19] J. Oliver, A. E. Huespe, J. Cante, An implicit/explicit integration scheme to increase computability of non-linear material and contact/friction problems, Computer Methods in Applied Mechanics and Engineering 197 (21-24) (2008) 1865–1889.

[20] G. Fotland, B. Haugen, Numerical integration algorithms and constraint formulations for an ALE-ANCF cable element, Mechanism and Machine Theory 170 (2022) 104659. doi:https://doi.org/10.1016/j.mechmachtheory.2021.104659.

[21] D. Baraff, A. Witkin, Large steps in cloth simulation, in: Proceedings of the 25th annual conference on Computer graphics and interactive techniques, 1998, pp. 43–54. doi:https://doi.org/10.1145/280814.280821.

[22] K.-J. Choi, H.-S. Ko, Stable but responsive cloth, ACM Transactions of Graphics 21 (3) (2002) 604–611. doi:10.1145/566654.566624.
URL https://doi.org/10.1145/566654.566624

[23] H. Sugiyama, A. A. Shabana, On the use of implicit integration methods and the absolute nodal coordinate formulation in the analysis of elastoplastic deformation problems, Nonlinear Dynamics 37 (3) (2004) 245–270. doi:https://doi.org/10.1023/B:NODY.0000044644.53684.5b.

[24] J. Hewlett, S. Arbatani, J. Kövecses, A fast and stable first-order method for simulation of flexible beams and cables, Nonlinear Dynamics 99 (2) (2020) 1211–1226. doi:https://doi.org/10.1007/s11071-019-05347-1.

[25] M. Servin, C. Lacoursiere, N. Melin, Interactive simulation of elastic deformable materials, in: SIGRAD 2006. The Annual SIGRAD Conference; Special Theme: Computer Games, no. 019, 2006.

[26] J. Baumgarte, Stabilization of constraints and integrals of motion in dynamical systems, Computer methods in applied mechanics and engineering 1 (1) (1972) 1–16. doi:https://doi.org/10.1016/0045-7825(72)90018-7.

[27] D. Negrut, R. Rampalli, G. Ottarsson, A. Sajdak, On the use of the HHT method in the context of index 3 differential algebraic equations

of multibody dynamics, in: International Design Engineering Technical Conferences and Computers and Information in Engineering Conference, Vol. 47438, 2005, pp. 207–218. doi:https://doi.org/10.1115/DETC2005-85096.

[28] S. Takehara, Y. Terumichi, K. Sogabe, Motion of a submerged tether subject to large deformations and displacements, Journal of System Design and Dynamics 5 (2) (2011) 296–305. doi:https://doi.org/10.1299/jsdd.5.296.